Optically excited Zeeman coherences in atomic ground states: Nuclear-spin effects

Dieter Suter

Institute of Quantum Electronics, Swiss Federal Institute of Technology (ETH) Zürich, CH-8093 Zürich, Switzerland

Optical experiments in alkali-metal atomic gases are usually interpreted in terms of the J=1/2 ground state, treating the electronic ground state as a degenerate two-level system. While this simplified level scheme has been quite successful in describing many experimental results, the nuclear spin can lead to significant modifications of the behavior. Apart from the obvious differences, such as the existence of hyperfine splitting, some more subtle effects are present that modify the dynamical as well as the equilibrium behavior of the system. An an example, the optical pumping process in the true atomic ground state is nonexponential and slower by at least an order of magnitude, compared to a hypothetical atom with nuclear spin zero. The limitations of the J = 1/2 model are analyzed theoretically and experimentally for atomic sodium, and experimental methods are demonstrated that can help disentangle the contributions from different hyperfine components.

I. INTRODUCTION

Vapors of alkali-metal atoms are used as model systems in many areas of atomic physics and quantum optics. Understanding the resonant interaction of polarized laser light with these atomic vapors is therefore a subject of rather general interest which has been renewed recently in the context of laser cooling of neutral atoms [1]. One of the unexpected results of these experiments was that the two-level approximation for the atoms, which takes only one ground and one electronically excited atomic state into account, fails to give an accurate description of the experimental results. Instead, it was found that population differences and coherences between the near-degenerate sublevels of the electronic ground state can have a large effect on the overall behavior of the system. In the past, the dynamics of these atomic- or sublevel coherences have been studied mainly in the context of optical-pumping experiments [2]. Apart from the interest in these systems in terms of the applications in laser cooling experiments, they are also interesting objects in their own right, e.g., due to the possibility to study nonlinear-optical phenomena at very low laser intensity.

In these experiments, the near-resonant polarized light propagating through the medium induces in general not only optical polarizations in the medium, but also population differences and coherences between these sublevels [3]. Such phenomena have been studied primarily in vapors of different alkali metals. Since a complete theoretical description of these systems can be rather involved, one usually resorts to various approximations, on the theoretical, as well as on the experimental side. An important experimental simplification is the elimination of inhomogeneous (Doppler) broadening, which can be achieved either by performing experiments in an atomic beam or by adding a buffer gas (typically a noble gas) to the sample cell. On the theoretical side, one usually simplifies the description by neglecting the complications due to the nuclear spin ($I = \frac{3}{2}$ in Na, $I = \frac{7}{2}$ in Cs). The

$J = \frac{1}{2}$ electronic ground state consists then of two degenerate substates and the electronically excited state of $2(^2P_{1/2})$ or $4(^2P_{3/2})$ substates. Due to the simplicity of this description, the resulting equations of motion can be solved analytically in many cases, and the model is very useful in giving qualitatively correct descriptions of many experimental observations.

The success of this relatively simple model in describing many experimental results should not obscure the fact that it is still a simplified model which cannot give a full description of all experimental findings. One particular example of an experimental finding that could not be explained in terms of this simple model was the observation of multiple echoes excited by a sequence of two laser pulses in the presence of an inhomogeneous transverse magnetic field [4]. These echoes are incompatible with the simple model, but could be explained successfully in terms of a more complete description that takes the hyperfine structure of the sodium ground state into account. For these and other optical-pumping experiments, the most important difference between the $J = \frac{1}{2}$ model and the actual systems with a nonvanishing nuclear spin are the presence of the hyperfine interaction and the larger multiplicity of the real systems. While some of the consequences, such as the existence of a hyperfine splitting, are rather obvious, others are more subtle and their influence on the experimental results may only appear in very specific situations. In order to assess the validity of the standard $J = \frac{1}{2}$ model, it is therefore important to consider also the less obvious deviations due to the nuclear spin.

Among the obvious consequences of the nonvanishing nuclear spin that will not be covered in this article are the presence of the hyperfine splitting and, associated with it, coherences between different hyperfine multiplets that evolve at the hyperfine splitting frequency, as well as optically produced population differences between the multiplets. We shall therefore concentrate on the evolution of the system within each multiplet, which is influenced
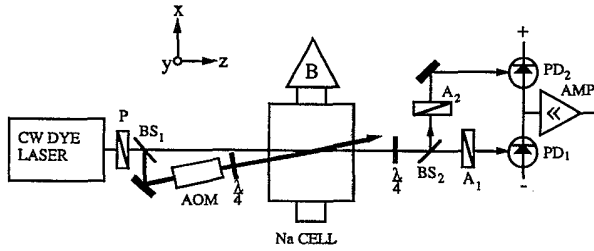
FIG. 1. Experimental setup for pump-probe experiments in a transverse magnetic field. P is the polarizer, BS is the beam splitter, AOM is the acousto-optic modulator, A is the analyzer, PD is the photodiode, and AMP is the amplifier.

by the nuclear spin in a much less obvious manner. All the consequences that will be discussed here do not vanish even in the limit of large homogeneous linewidth and small hyperfine coupling.

A typical experimental setup for the investigation of such effects, based on the principle of "quantum beats in forward scattering" [5], is shown schematically in Fig. 1. The atomic medium (Na vapor in the experimental examples) is evaporated in a heated glass cell in the presence of a buffer gas. A homogeneous magnetic field is applied perpendicular to the direction of the laser beams. A circularly polarized pump beam creates the sublevel coherence in the medium. Its intensity can be controlled with an acousto-optic modulator. The probe beam is derived from the same cw ring dye laser and linearly polarized; it overlaps with the pump beam in the probe region with a small angle of intersection ($<1°$). Behind the sample region, the difference in absorption or dispersion between right and left circularly polarized light is measured.

Before we can discuss some of the effects of the nuclear spin, we need to specify the reference system by giving a brief summary of the spinless model. More detailed descriptions can be found elsewhere [6,7].

II. THE $J = \frac{1}{2}$ MODEL

Figure 2 shows a simplified model system of the D_1 transition of atomic sodium with a $J = \frac{1}{2}$ ground state
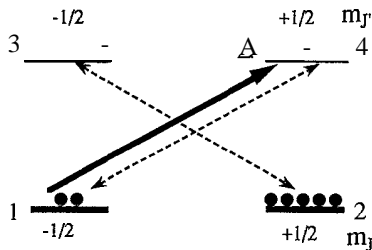
FIG. 2. Simplified model system of the D_1 transition in atomic sodium with a $J = \frac{1}{2}$ ground state and a $J' = \frac{1}{2}$ excited state. The solid arrow indicates optical pumping with a circularly polarized laser beam and the dashed arrows show how the resulting ground-state polarization can be detected optically with a linearly polarized probe beam.

and a $J' = \frac{1}{2}$ excited state. The solid arrow indicates optical pumping with a circularly polarized laser beam and the dashed arrows indicate how the resulting ground-state polarization can be detected optically with a linearly polarized probe beam. Typical experimental conditions for such experiments include the addition of buffer gas to the sample cell in order to suppress the Doppler broadening of the optical transition and increase the time during which the atoms remain inside the laser beam. A side effect of this buffer gas is the resulting collisional broadening of the resonance line: the optical coherences are destroyed rapidly by the atomic collisions. As a consequence, not only the optical coherences, but also the population of the excited state, remain relatively low. For many cases, the signal obtained from the probe beam is therefore determined by the ground state while the electronically excited state need not be taken into account. It is therefore advantageous to consider the dynamics of a subsystem consisting only of two substates of the electronic ground state.

The density operator of the ground-state subsystem can be parametrized in the usual Feynman-Vernon-Hellwarth picture [8]. It is therefore customary to define a magnetization or spin vector m as

$$\mathbf{m} = (\rho_{12} + \rho_{21}, -i(\rho_{12} - \rho_{21}), \rho_{22} - \rho_{11}) . \tag{1}$$

In order to describe an experiment of the type shown in Fig. 1, we use a coordinate system whose z axis is parallel to the direction of the laser beam, while the x axis is parallel to the magnetic field $\mathbf{B} = (B, 0, 0)$. We neglect the probe laser beam and analyze the dynamics of the atomic system under the influence of the pump beam and the magnetic field. In terms of this magnetization vector, the equations of motion can be described with the relatively simple equation

$$\dot{\mathbf{m}} = \mathbf{\Omega} \times \mathbf{m} - \gamma_{\mathrm{eff}} \mathbf{m} + \mathbf{P} . \tag{2}$$

The first term on the right-hand side corresponds to a precession of the magnetization vector m around the effective field $\mathbf{\Omega} = (\Omega_L, 0, \overline{\Delta} P_+)$, where $\Omega_L = (\mu_B g B)/\hbar$ represents the Larmor frequency due to the magnetic field B, μ_B denotes Bohr's magneton, and g is the Landé factor. The z component of the effective magnetic field, $\overline{\Delta} P_+$, is a virtual magnetic field due to the light-shift effect. It is proportional to the normalized laser frequency detuning $\overline{\Delta} = \Delta/\Gamma_2$, where $\Delta = \omega - \omega_0$ is the difference between the laser frequency ω and the atomic resonance frequency ω_0, and Γ_2 is the decay rate of the optical coherences. It is also proportional to the optical pump rate P_+:

$$P_+ = \frac{|\omega_1|^2}{\Gamma_2(1 + \overline{\Delta}^2)} , \tag{3}$$

where $\omega_1 = \mu_e E_+ / 2\hbar$ represents the optical Rabi frequency. This light-shift-induced virtual magnetic field points along the direction of the laser beam, so that the total field lies in the xz plane.

The second term of Eq. (2) describes the decay of the ground-state magnetization with a decay rate

$\gamma_{\text{eff}} = \gamma_0 + P_+$. The two contributions to the total decay rate that are included here are the diffusion contribution γ_0, which describes the effect of atoms drifting out of the laser beam, and the effect of the optical pumping P_+. The last term of Eq. (2), $P = (0, 0, P_+)$, describes the magnetization that is created by the optical-pumping process parallel to the z axis (the direction of the laser beam).

This equation of motion is quite analogous to the well-known Bloch equation [9] describing the precession of a spin in a magnetic field. The solutions of the Bloch equations are well known in this case and correspond to a precession of the magnetization vector around the effective field $\mathbf{\Omega}$, damped with the relaxation rate γ_{eff} towards a nonthermal equilibrium state that is determined by the intensity and detuning of the laser field, the Larmor frequency Ω_L, and the diffusion rate γ_0 [7]. This straightforward solution allows therefore not only numerical integration of the equations of motion, but also analytical discussions which make it relatively easy to obtain at least a qualitative idea of the dynamics occurring at the atomic level.

The evolution of the atomic system can be monitored with a linearly polarized probe beam that basically compares the populations of the two ground-state sublevels: the two dashed arrows in Fig. 2 correspond to the circularly polarized components of the probe beam which interact with the two σ transitions. The medium exhibits therefore circular birefringence and circular dichroism proportional to the difference of the two populations. With a polarization-selective detection scheme, as shown in Fig. 1, it is therefore possible to measure this population difference directly via the difference in absorption or dispersion of the circularly polarized components. The sensitivity of this detection depends of course on the laser detuning; in the case of absorptive detection, the sensitivity is highest on resonance, while the maximum occurs at $\overline{\Delta} = \pm 1$ in the case of dispersive detection.

It is clear that the simple model, as it was outlined in this section, cannot accurately describe experiments performed, e.g., on the ground state of atomic cesium at low buffer gas pressures, where the hyperfine interaction is well resolved and optical hyperfine pumping is important. In the case of Na at moderate buffer gas pressures, however, the model has been rather successful and it is often argued that the fact that the hyperfine interaction is not resolved in the spectrum, is a good indication that the approximation holds. In the following, some less obvious consequences are pointed out, that persist even in the limit of large homogeneous linewidths.

III. OPTICAL PUMPING

One of the less obvious effects of the nuclear spin is the modification of the optical pumping rate. As will be seen, the optical-pumping process in systems with nonzero nuclear spin is nonexponential, and the time scale is more than an order of magnitude longer compared to a system with no nuclear spin under the same experimental conditions. It is the purpose of this section to demonstrate this theoretically and experimentally by connecting the optical-pumping process to directly observable quantities,

such as the laser intensity, and demonstrate the differences that are due to the nuclear spin.

We start by calculating the matrix elements of the electric dipole moment. The absolute value can be obtained, e.g., from the excited-state lifetime. For the $^3P_{1/2}$ state of Na, the lifetime is $T_1 = 16$ ns. We calculate the dipole moment for the D_1 transition as [10]

$$3d^2 = \frac{1}{T_1} \frac{3\pi\epsilon_0 \hbar c^3}{\omega_0^3}, \tag{4}$$

still within the $J = \frac{1}{2}$ model. The factor of three takes into account the fact that the spontaneous decay rate includes contributions from the $\sigma_\pm$ and π transitions. In order to connect the measured laser intensity with the atomic interaction energy, we calculate the peak amplitude of a traveling electromagnetic wave of intensity I as $E_0 = (2Iz_0)^{1/2}$ (linear polarization) or $E_0 = (Iz_0)^{1/2}$ (circular polarization), where $z_0 = (\mu_0/\epsilon_0)^{1/2}$ In the rotating frame, the (constant) field strength becomes for circularly polarized light $E^r = E_0$ and the interaction energy is therefore $E_0 d = (Iz_0)^{1/2} d = 2\omega_1$ where ω_1 represents the Rabi flopping frequency. In the framework of the $J = \frac{1}{2}$ model, the optical pump rate $P_{1/2}$, defined via

$$\frac{d}{dt}(\rho_{22} - \rho_{11}) = P_{1/2}[1 - (\rho_{22} - \rho_{11})] \tag{5}$$

is then, according to Eq. (3), with $\overline{\Delta} = 0$

$$P_{1/2} = \frac{E_0^2 d^2}{\hbar^2 \Gamma_2}. \tag{6}$$

If the nuclear spin is taken into account, the situation is of course more complex. In order to define the notation, Fig. 3 shows the ground-state level system of Na with a numbering of the different sublevels as it will be used in the following. The total absorption of the Na ground state remains of course the same, as long as the system is in internal equilibrium. However, as the population differences build up, the behavior becomes more complex, since there is no longer a single Rabi frequency in the system.

For the quantitative calculation, we shall restrict ourselves to the case of a pressure-broadened system, where the collision-induced reorientation in the excited state is fast. Assuming for the moment on-resonance irradiation for both hyperfine multiplets, the absorption rate of the individual sublevels is
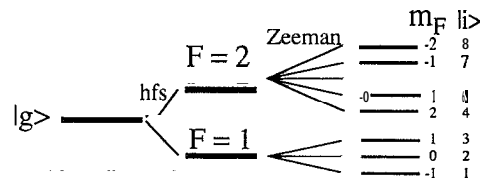
FIG. 3. Level system of the ground state of atomic sodium taking the hyperfine structure into account.

Level i	1	2	3	4	5	6	7	8
Rate k_i/k_0	1	2	3	0	1	2	3	4

where $k_0 = P_{1/2}/(2I+1)$.

The repopulation rate is obtained from the conservation of the total population. The equation of motion for the difference is then

$$\dot{\rho}_{ii}(t) = -k_i\rho_{ii}(t) + \frac{1}{8}\sum_{i=1}^{8} k_i\rho_{ii}(t) \ . \tag{7}$$

Starting from thermal equilibrium ($\rho_{ii} = \frac{1}{8}$), irradiation with σ_+ light will therefore lead to an initial rate of

$$\dot{\rho}_{ii}(0) = \frac{k_0}{4} - \frac{k_i}{8} \ , \tag{8}$$

which takes the values of $P_{1/2}/32\,(1,0,-1,2,1,0,-1,-2)$ for the eight Na ground states. If the optical pumping is the only process driving the system, the equation of motion can then be integrated easily, as shown in Fig. 4, where the evolution of the eight sublevel populations is displayed as a function of time. The system is assumed to be initially in thermal equilibrium. As the laser beam is turned on, the three populations with the weakest coupling to the pump laser (1,4,5) start to increase, while two (2,6) remain constant, and the remaining three (3,7,8) decrease. Over a longer time, however, all populations decay towards zero, with the only exception of the $m_F = 2$ level, the only substate not coupled to the field. In the long-time limit, all atoms end up in this single substate, if relaxation effects can be neglected.

In an actual experiment, it is of course often not possible or not interesting to observe these sublevel populations individually. The actual signal, which is typically the difference in absorption or dispersion of the two circularly polarized components, is then a weighted superposition of all sublevel populations. Since these populations evolve at different rates, the overall signal becomes nonexponential.

In order to confirm this prediction experimentally under well-defined conditions, care was taken to homogeneously illuminate the sample with a well-defined intensity. This was achieved by using a pump laser beam consider-
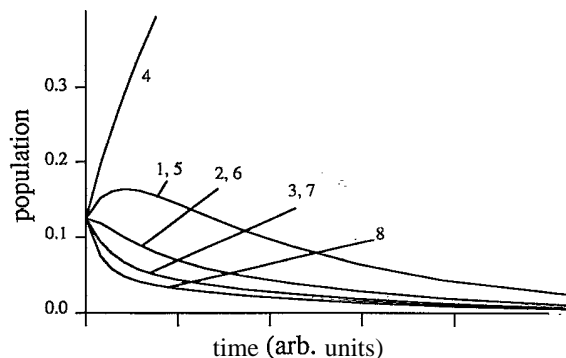
FIG. 4. Evolution of the individual populations of the Na ground state. The labeling of the different curves refers to Fig. 3. The individual curves were calculated according to Eq. (7).
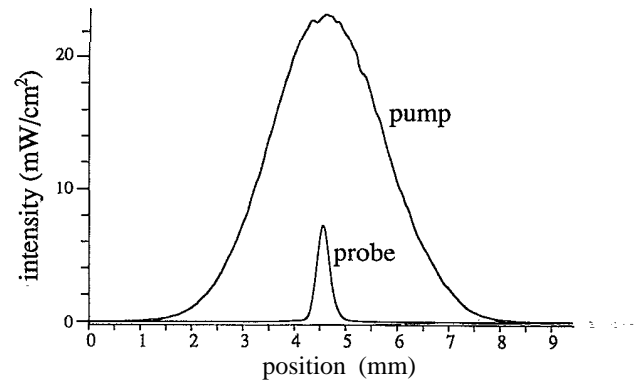
FIG. 5. Intensities of the pump and probe beams (recorded separately) at the center of the sample cell. Both beam profiles are approximately Gaussian.

'ably wider than the probe beam, so that the observed signal stems only from the central part of the (Gaussian) pump beam which is relatively homogeneous over the diameter of probe beam. The situation was checked by measuring the cross sections of both pump and probe beams, at the center of the sample cell, as shown in Fig. 5. The two beam profiles were recorded with a photodiode array and the measured signal was scaled such that the integrated pump beam power became equal to the measured value of 1.8 mW. The rest of the experimental setup was as shown in Fig. 1.

The resulting signal is shown in Fig. 6, together with the theoretical signals calculated for the $J = \frac{1}{2}$ model [Eq. (5)] and the full Na level system [Eq. (7)]. As shown in Fig. 5, the intensity at the center of the probe beam was 23.2 mW/cm^2, corresponding to an interaction energy $E_0 d/\hbar$ of 3.5×10^7 rad/sec. For the optical dephasing rate we use a value of $\Gamma_2 = 9.4 \times 10^9$ rad/sec, as determined from the absorption spectrum. These values result in an optical-pumping rate of $P_{1/2} = 1.3 \times 10^5$ sec^{-1}, or a
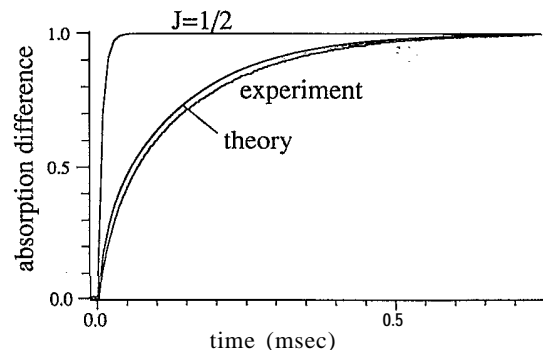
FIG. 6. Evolution of the signal as a function of time when a circularly polarized pump beam is turned on at $t = 0$. The curve labeled "experiment" represents the experimental signal obtained with the setup of Figs. 1 and 5. The other two curves are theoretical functions calculated within the $J = \frac{1}{2}$ model and the full Na ground state for the experimental parameters used in the actual experiment and no adjustable parameters.

time constant $1/P_{1/2}=7.7\,\mu sec$, much shorter than the observed time scale. The curve calculated for the full system, on the other hand, reproduces the experimental signal quite well, especially the overall shape of the signal which is clearly nonexponential., The agreement becomes almost perfect (not shown in the figure) if we assume that the true optical beam power is 20% smaller than the measured value; such a discrepancy would be well within the experimental uncertainty of our measurements, especially because the reflection losses from the entrance window to the sample cell could not be taken into account. The discrepancy between the two nonexponential curves and the simple exponential predicted by the $J=\frac{1}{2}$ model is rather obvious in the figure. Apart from the qualitative difference, the different times scales are also rather surprising: the time required to reach 50% polarization is an order of magnitude longer for the actual level system than would be predicted from the $J=\frac{1}{2}$ model.

IV. LARMOR PRECESSION

One of the well-known consequences of the hyperfine interaction is the reduction of the g factor: for the true eigenstates, it is reduced by the multiplicity of the nuclear spin states, $g_F=g_J/(2I+1)$. This represents of course a low-field approximation which is valid as long as the Zeeman interaction is small compared to the hyperfine interaction. This is usually the case under the typical experimental conditions that include magnetic fields no larger than a few gauss. However, even at these fields, deviations from the idealized description with a single Larmor frequency are observable and can actually be utilized to extract more information on the internal state of the atomic system.

The main differences between the $J=\frac{1}{2}$ model and the actual behavior can be traced to two different effects, the second-order Zeeman interaction, and the nuclear Zeeman effect. The former, which represents the second term in the Taylor expansion of the electron Zeeman interaction with respect to the magnetic field, increases with the square of the magnetic field strength and the square of the m_F quantum number. It leads therefore to a separation of the Larmor frequencies of the different sublevel transitions within each hyperfine multiplet.

The nuclear Zeeman effect is several orders of magnitude smaller than the electron Zeeman effect. Nevertheless, it can readily be observed even at relatively low-field strengths of the order of a few gauss. Since the hyperfine multiplets differ essentially by the relative orientation of the electron and nuclear angular momentum, the nuclear Zeeman effect shifts the Larmor frequencies of the two multiplets in opposite direction. As a result, all the possible transition frequencies in the ground state of sodium are nondegenerate and can be distinguished if the field strength exceeds a value of approximately 1 G, depending on the width of the resonances.

An example of how this distinction can be achieved is represented in Fig. 7. In order to record this spectrum, the Na cell was placed in a transverse magnetic field of 0.7 mT, as shown in Fig. 1. The lower part of the figure shows the different energy levels as a function of the mag-
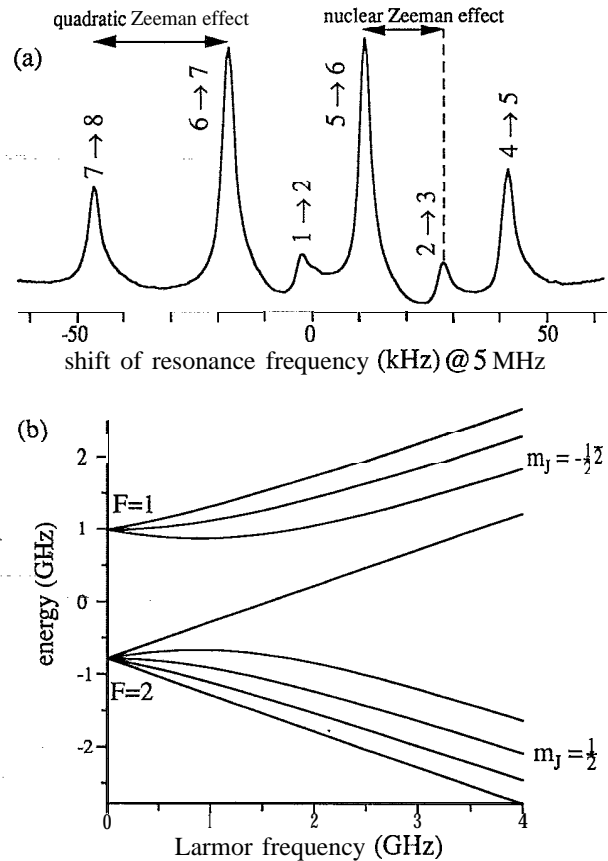
FIG. 7. Experimental spectrum demonstrating how the various Zeeman coherences within the two hyperfine multiplets can be distinguished. The labeling of the transitions refers to Fig. 3. The experimental setup used was that of Fig. 1, with a magnetic field strength of 0.7 mT.

netic field strength. All the experiments discussed here were performed for magnetic field values very close to the origin. The upper part shows a spectrum of the sublevel transitions, labeled with the indices of the relevant sublevels, as defined in Fig. 3. For this experiment, the Na atoms were excited with a pulse of circularly polarized light whose amplitude was modulated with a frequency near the Larmor frequency of the atoms in order to efficiently pump the system [7]. After the atoms had reached a steady state, the pump laser was switched off and the resulting polarization of the atoms was allowed to precess freely in the magnetic field. This precession was detected with a weak, linearly polarized probe beam, using phase-sensitive detection at the modulation frequency. The digitized signal of this free induction decay was Fourier transformed. The six resonance lines that can be seen correspond to the six possible transitions with $|\Delta m_F|=1$ within the two hyperfine multiplets.

The fact that only six out of the 13 possible Zeeman transitions are observed does not imply that the other transitions are not excited. In general, all possible transitions are excited, but the setup used here, which measures the circular birefringence, is sensitive only to transitions

between adjacent states, the magnetic dipole transitions that are also observed in conventional magnetic resonance experiments. The other transitions, the so-called multiquantum transitions, can be observed either with different experimental setups or by transferring the coherence generated in these transitions to other transitions that can be observed directly [4].

V. DETECTION

The experiments which we consider here are all based on the concept of "quantum beats in forward scattering" [5]. In these experiments, a linearly polarized laser beam propagates through the medium and is subjected to a polarization-selective detection behind the sample. The resulting signal basically reflects differences in the complex index of refraction of the sample for the eigenpolarizations of the light. For a medium consisting of $J = \frac{1}{2}$ atoms with no nuclear spin, the eigenpolarizations are very close to the circular polarizations-the differences are of the order of the susceptibility of the medium, i.e., typically smaller than 10^{-5}.

The main difference between the $J = \frac{1}{2}$ ground state and the true atomic ground state is the existence of sublevel transitions with $|\Delta m_F| = 2$. For this type of A transition, coherence between the sublevels gives rise to linear birefringence. However, the size of these effects scales with the ratio of the excited-state hyperfine splitting to the homogeneous optical linewidth. As a first step from the $J = \frac{1}{2}$ model to the true atomic ground state, we consider therefore again the circular birefringence and dichroism induced by the nonthermal population of the ground-state sublevels. The size of the effect is proportional to the sublevel polarization and the susceptibility of the unpolarized sample and shows therefore the usual dispersion and absorption behavior. Since the optical transition frequencies for the two hyperfine multiplets differ, we expect that the corresponding population differences contribute to the overall signal with a different frequency dependence. This difference is of course readily observable in the case of Cs or rubidium, where the hyperfine splitting is usually well resolved.

In the case of Na, where the hyperfine splitting is not resolved if a few hundred Torr of buffer gas is present in the sample, the effect is less obvious and actually cannot be observed under many experimental conditions, since the signal contributions overlap. However, as we have seen in Sec. IV, the signal contributions can be distinguished by their Larmor frequency. This makes it possible to observe a different dependence of the two components on the laser frequency. Since the detection sensitivity is not the only quantity that depends on the laser frequency, a straightforward laser frequency scan may not show the expected frequency shift between the two components. The problem is basically that the internal state of the system is affected simultaneously via the changes of the pump laser frequency, if, as with the setup of Fig. 1, the pump laser beam is derived from the same laser as the probe beam. Ideally, pump and probe beams should therefore be derived from separate lasers, so that the pump beam frequency can remain fixed, while the
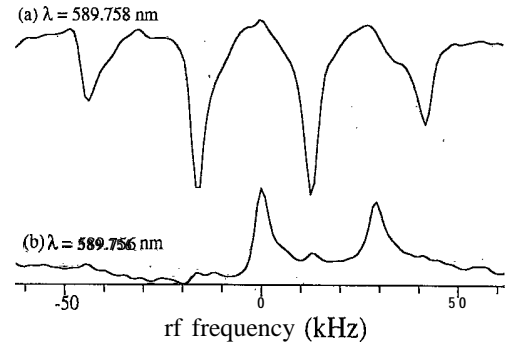
FIG. 8. Sublevel spectra recorded at two different laser wavelengths near the Na D_1 transition with dispersive detection. The wavelengths were set to the pressure-shifted transitions $F = 1 \rightarrow F' = 1, 2$ (a) and $F = 2 \rightarrow F' = 1, 2$ (b).

probe beam measures the dispersion properties of the induced birefringence.

Even with a single laser, however, a clear distinction remains possible if dispersive detection at a field strength of a few gauss is used. Via the scheme outlined in the preceding section, it is then possible to distinguish the different components. The dispersive detection scheme allows a precise determination of the resonance frequency, where the detection sensitivity vanishes. The result of such a measurement is shown in Fig. 8. For the upper spectrum, the laser wavelength was set on resonance with the $F = 1 \rightarrow F' = I, 2$ transition. Since the detection sensitivity is antisymmetric with respect to the laser detuning, the sensitivity for the $F = 1$ contributions has a zero crossing at this wavelength and only the $F = 2$ components contribute to the signal. The lower spectrum was recorded at the wavelength of the $F = 2 \rightarrow F' = 1, 2$ transition and shows therefore only the $F = 1$ components.

VI. SUMMARY AND CONCLUSION

The main purpose of this article was an investigation into the limits for the validity of the $J = \frac{1}{2}$ model used for the description of the ground-state dynamics of alkali-metal atoms. This mode is used extensively and successfully for the description of the interaction of atomic gases with laser radiation in the cases where the hyperfine interaction can be neglected. The main justification for this approximation is often the argument that the hyperfine splitting is hidden underneath the pressure-broadened line. Of course, the very success of this model already shows that this assumption is often justified, and it cannot be the purpose of this article to prove it invalid. Instead, we have addressed the question of *under what circumstances* the approximation is well justified and when it has to be modified.

Among the consequences of the nonvanishing nuclear spin, some are rather obvious and need not be addressed here. Among the less obvious is the modification of the optical-pumping rate. In real systems, the optical-pumping process is not even characterized by a single rate, but, in the case of the Na ground state, by a super-

position of eight different rates. The overall process that is usually observed in an experiment is therefore nonexponential and proceeds much more slowly than it would under the same experimental conditions for hypothetical atoms without nuclear spin. It should again be stressed here that this behavior does not depend on the relative size of hyperfine splitting and homogeneous linewidth, but persists even under conditions of arbitrarily high buffer gas pressure; in fact, the size of the hyperfine coupling does not even enter the theoretical calculation that is compared with the experimental data in Fig. 6 and may therefore perfectly well be zero without affecting the result.

A useful experimental method for the distinction of signal contributions from the different hyperfine multiplets consists in applying a transverse magnetic field of a few gauss. Due to first- and second-order electron Zeeman effect and nuclear Zeeman interaction, the different sublevel coherences precess then with different frequencies and can thereby be distinguished experimentally. This procedure allows, one, e.g., to show that the detection sensitivities for the different hypertine components have different dependencies on the laser frequency.

In conclusion, the $J = \frac{1}{2}$ model seems alive and well, provided some care is taken when quantitative information is requested. Taking into account the nonexponential optical-pumping process may be specially important in nonlinear experiments with high-intensity radiation or optical cavities [6]. In these cases, the description with a single pumping rate needs to be modified. One possible solution that could preserve the simplicity of the usual model to a large degree might be to retain the two-level description of the ground-state dynamics but use a pump rate that depends on the internal state of the system: the larger the polarization of the system, the smaller the pump rate.

For the experimental investigation of these deviations, methods have been developed that may be helpful for the investigation of the limitations of the model in specific situations of interest, especially in conjunction with numerical integration of the equations of motion for the full level system. Depending on the experimental parameters, the equations of motion can, even for the full level system, remain simple enough to make numerical simulations feasible even on small personal computers. These numerical experiments can then give precise indication where the hyperfine interaction is important.

ACKNOWLEDGMENTS

[1] See, e.g., S. Chu, Science 253, 861 (1991), and references therein.
[2] See, e.g., A. Kastler, Science 158, 214 (1967), and references therein.
[3] See, e.g., D. Suter and J. Mlynek, Adv. Magn. Opt. Reson. 16, 1 (1991), and references therein.
[4] D. Suter, M. Rosatzin, and J. Mlynek, Phys. Rev. Lett. 67, 34 (1991).
[5] W. Lange and J. Mlynek, Phys. Rev. Lett. 40, 1373 (1978).
[6] F. Mitschke, R. Deserno, W. Lange, and J. Mlynek, Phys. Rev. A 33, 3219 (1986).
[7] D. Suter and J. Mlynek, Phys. Rev. A 43, 6124 (1991).
[8] R. P. Feynman, F. L. Vernon, and R. W. Hellwarth, J. Appl. Phys. 28, 49 (1957).
[9] F. Bloch, Phys. Rev. 70, 460 (1946).
[10] See, e.g., W. Demtröder, Laser Spectroscopy (Springer, Berlin, 1991).